JOURNAL OF PROPULSION AND POWER
Vol. 15, No. 5, September–October 1999

Aerodynamic Effects on Blade Vibratory Stress Variations

James A. Kenyon* and Douglas C. Rabe†
U.S. Air Force Research Laboratory, Wright–Patterson Air Force Base, Ohio 45433-7251
and
Sanford Fleeter‡
Purdue University, West Lafayette, Indiana 47907

Blade-to-blade variations in blade resonant frequencies, known as mistuning, and how these variations are related to vibratory stress amplitude and viscous damping variations were investigated for an integrally bladed disk, or blisk. Blade response to an inlet total pressure distortion was measured using dynamic strain gauges with the blisk at operating conditions. In addition, a reduced-order analytical model of the blisk was used to predict the blade resonant stress variations. The measured stress variations were found to be strongly influenced by unsteady aerodynamic coupling. Blade structural mistuning and mechanical coupling through hub motion were determined to have only a minor influence on blade-to-blade stress variations. Stress distribution patterns at resonance and at constant speeds above and below resonance suggested a relationship between stress variations and unsteady aerodynamics. To support this, aerodynamic damping variations measured at resonance were shown to correspond roughly to stress variations. Experimental results were compared to the predicted variations from the reduced-order model. Results from the model indicated that unsteady aerodynamic coupling played an important role in the mistuned response of the blisk.

Nomenclature

C = engine order of excitation, or hub nodal diameters
M = Mach number
N = number of blades on rotor
Q = dynamic magnification factor
ζ = viscous damping ratio
σ_B = interblade phase angle

Introduction

MISTUNING in a compressor rotor may contribute to engine high-cycle fatigue by significantly increasing individual blade vibratory stress amplitudes, which in turn decreases the number of cycles to failure for subject blades. Mistuning arises when minor variations in the components of a periodic system lead to mode localization and is characterized by strong resonant vibrations in a small region of the rotor. Localization means that prediction, measurement, and control of resonance become more complex and may also result in increased stress amplitudes in comparison to a tuned response. In a compressor rotor the effect of mistuning on vibration amplitude is evident as significant variations from blade to blade with particular blades responding more vigorously than the mean response.

Numerous studies of traditional bladed-disk assemblies, both experimental and analytical, have focused on understanding the physics involved in mistuning.[1–5] These have primarily involved rotors in a static condition. Probabilistic studies have also been accomplished to try to develop methods of predicting mistuning in rotor design.[6,7] Other approaches, such as finite element analysis, have attempted to model more closely real system dynamics. Most finite element models of rotors employ cyclic symmetry, thereby eliminating the possibility of mistuning. Some models have been developed to investigate mistuning, but they tend to be computationally cumbersome.[8,9] One of the most recent techniques, developed by Ottarsson et al.[10] and Kruse and Pierre[11] uses a reduced-order method that introduces variations into the calculations for cyclically symmetric finite element models to yield mistuning effects, thereby reducing computational requirements.

Experimental mistuning research on rotating machinery has been limited. Griffin[12] measured mistuning for a low-speed, low-frequency bladed-disk assembly using strain gauges. He focused particularly on probabilistic results, which he correlated with an analytical model developed in the same study. He found that the largest stress amplitudes occurred for blades that vibrated near the tuned-disk frequency, which he defined as the frequency at which the bladed disk would respond if the blades were all tuned.

Modern compressor rotors often use a blisk design. A *blisk* is an integrally bladed disk in which the disk and blades are machined from a continuous piece of material, often resulting in a higher degree of tuning in the rotor. Because previous studies have generally focused on bladed-disk assemblies rather than monolithic blisks, further investigation of mistuning in a blisk configuration is vital to understanding its effects in a modern compressor rotor.

The objective of this paper is to provide a comprehensive account of natural frequency and vibratory stress variations for a single blisk mode. A rotor was accelerated through its first resonant blade mode, the first flex (1F) mode, which was excited by a 3/rev inlet total pressure distortion. Data from dynamic strain gauges quantified resonant frequencies, vibratory stress amplitudes, and viscous damping so that blade-to-blade variations in these parameters could be evaluated. The variations found for each of these parameters were correlated to determine the dependence between them and to gain insight into why they occurred. Stress variations at the forcing frequency for steady-state dwells above and below the 1F resonance were also examined. Finally, the blisk was analyzed using the reduced-order model of Refs. 10 and 11, with the results compared to experimental data to evaluate the role of unsteady aerodynamic coupling.

Experimental Configuration

The experiment investigated mistuning effects in the first stage of a two-stage compressor, shown schematically in Fig. 1. This rotor is a blisk configuration with 16 airfoils and an integral stub shaft constructed of Ti-6-4. The blisk is an advanced design composed of low aspect ratio blades, as described by the geometric parameters shown in Table 1.

Received 11 August 1998; revision received 3 March 1999; accepted for publication 27 March 1999.

*Aerospace Engineer, Propulsion Directorate, AFRL/PRTE, 1950 Fifth Street, Building 18D. Member AIAA.
†Director, Turbine Engine Research Center, Propulsion Directorate, AFRL/PRTX, 1950 Fifth Street, Building 18D. Member AIAA.
‡McAllister Distinguished Professor of Mechanical Engineering, School of Mechanical Engineering. Associate Fellow AIAA.

Table 1 Rotor 1 geometric parameters

Parameter	Value
Average aspect ratio	1.22
Rotor tip radius, cm	35.24
Inlet radius ratio	0.33
Average radius ratio	0.47
Average tip solidity	1.50
Maximum thickness/chord	0.028

Table 2 Rotor 1 performance parameters

Parameter	Design condition	Test condition
Percent rotor speed	98.6	68.5
Adiabatic efficiency, %	88.9	81.6
Total pressure ratio	2.50	1.59
Total temperature ratio	1.30	1.18
Tip speed, m/s	483.5	335.8
Mass flow, kg/s	71.8	45.9

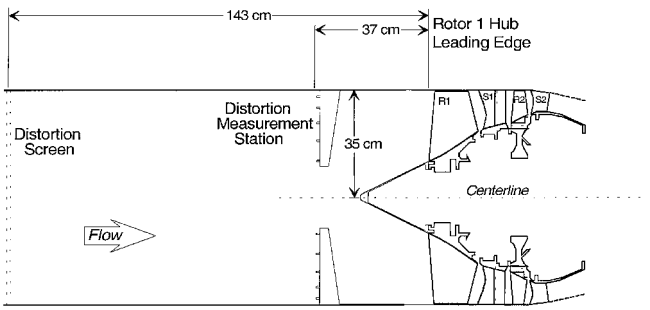

Fig. 1 Test compressor schematic.

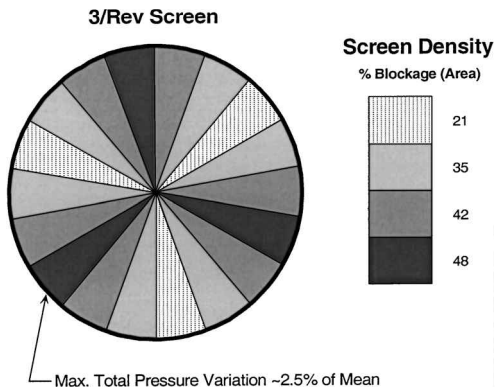

Fig. 2 Inlet distortion screen.

The aerodynamic design pressure ratio and mass flow for rotor 1 occur at a corrected speed of 13,288 rpm. For this experiment mistuning effects were evaluated near the first blade resonant crossing, the 1F mode, at a frequency of approximately 435 Hz. This mode occurs at a mechanical speed near 8700 rpm with a 3/rev disturbance. The performance parameters of the rotor at design condition and at the test condition of this study are shown in Table 2. At the design point the rotor relative airflow is supersonic at 45% span for inlet temperatures near 300 K. For the test condition investigated in this report, the flow is subsonic throughout $M \approx 0.8$–0.9.

The forcing function used to excite the 3/rev resonant test condition was produced by an inlet total pressure distortion introduced using a meshed screen mounted in the compressor inlet, as shown in Fig. 1. The porosity of the screen was incremented around the compressor circumference to produce a roughly sinusoidal forcing function. A diagram of the screen showing this mesh density can be seen in Fig. 2.

The distortion pattern was mapped 37 cm upstream from the compressor face using a distortion rake consisting of total pressure

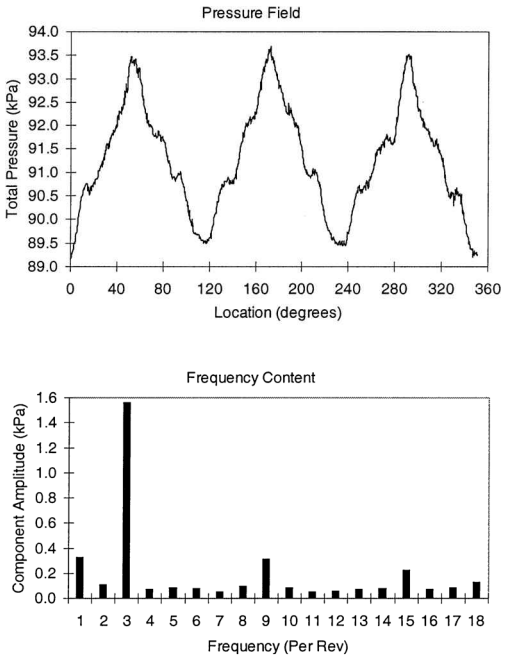

Fig. 3 Characterization of forcing function.

probes at five radial immersions in the flow, as shown in Fig. 1. The distortion screen was rotated with the rake fixed so that a circumferential pressure distribution consisting of 889 measurements was recorded at each immersion. The mean pressure distribution and corresponding frequency content of the aerodynamic forcing function are shown in Fig. 3. The screen produced a maximum total pressure variation of approximately ±2.5% of the circumferential mean. The primary component of the inlet pressure field was the intended 3/rev forcing function, but other excitations were present as well, as seen in Fig. 3. These had little effect on rotor response at the 1F crossing. The distortion measurement rake was removed before obtaining the strain-gauge data presented here to eliminate any blade response caused by wakes generated by the rake.

Instrumentation and Data Acquisition

Strain instrumentation consisted of dynamic strain gauges applied at the root of each of the 16 rotor blades. The uncertainty of these gauges in stress amplitude measurement at the 1F mode was estimated at approximately ±6%, based on signal conditioning equipment specifications and the methods of Nichol.[13]

Campbell diagrams were generated for all of the strain gauges during accelerations through resonance, from 8100 to 9100 rpm mechanical speed. These speed increases were executed at a rate of approximately 30 rpm/s, which was rapid enough to avoid damaging the rotor but still allowed the acquisition of useful peak resonance data. Figure 4 shows one of the Campbell diagrams produced during the experiment. The processor sampled data at a rate of 30 kHz and performed a fast Fourier transform (FFT) on each signal to determine the frequency response of the strain gauge and the amplitude of each frequency component. The frequencies and corresponding stress amplitudes were plotted on the Campbell diagram as a function of rotor mechanical speed. The Campbell diagram in Fig. 4 shows a strong response at the 1F mode. Additional responses to other modes can also be seen near a frequency of 1200 Hz. These were caused by the additional forcing function components already mentioned in the discussion of the 3/rev screen. The additional responses had a negligible impact on the 1F response. Resonant frequencies and peak stress amplitudes for each blade were determined at the 1F mode directly from the Campbell diagrams.

In addition to Campbell diagrams, strain-gauge signals were recorded on analog tape. Twenty seconds of recorded data for off-resonant operation at 8100 and 9100 rpm were sampled at a rate of 2.5 kHz. An FFT of each digital signal determined the primary

Table 3 Compressor mass flows

Operating line	Mass flow, kg/s
WOD	45.2
NOL	44.8
PE	44.1
NS	41.9

Table 4 Rotor mean resonant stresses and frequencies

Operating line	Mean stress, kPa	Mean frequency, Hz
WOD	145,335	435.8
NOL	141,908	435.5
PE	137,334	435.3
NS	126,115	435.0

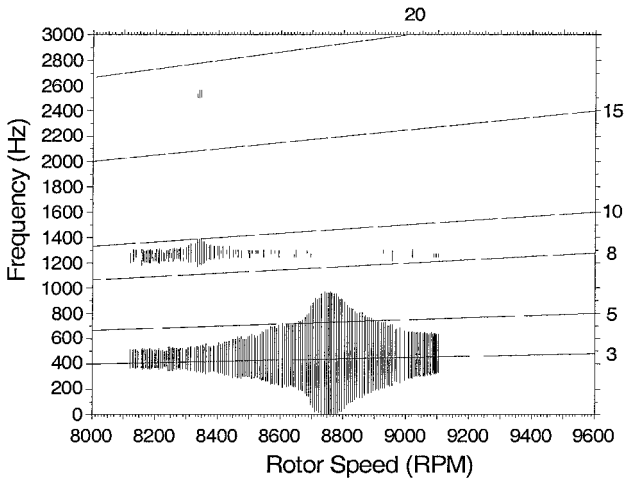

Fig. 4 On-line Campbell diagram.

response frequency and amplitude for each blade at the off-resonant conditions above and below resonance.

Testing took place on four different compressor operating lines. The throttle settings for these operating lines were defined by corrected mass flow at 8100 rpm. Mass flow was adjusted using a close-coupled discharge valve at the compressor exit. The conditions consisted of the maximum throttle area or wide open discharge (WOD), the nominal operating line (NOL), peak efficiency (PE), and near stall (NS). Mass flows for the operating lines are shown in Table 3.

Experimental Results

Examination of response frequencies and peak stresses at resonance allow for evaluation of mistuned response in the blisk. Figure 5 shows the circumferential distribution of peak stress and resonant frequency variations. The variations are presented as a percentage of the mean for each operating condition. The mean stresses and frequencies for each operating line are provided in Table 4 for reference.

The data in Fig. 5 indicate that the blisk is essentially tuned. The frequency varied by less than 0.7% of the mean for all blades on all operating lines. However, the peak stresses varied by up to 26% of the mean along NOL, with standard deviations ranging from 11.4% along WOD to 12.4% along NOL. Closer examination also shows that the distribution patterns around the rotor circumference are not the same for frequency and stress, thus demonstrating little correlation between these parameters. Blades that respond below the mean frequency do not show a tendency for either higher or lower than mean peak stress. Because natural frequency is a direct measurement of blade structure, this lack of correlation indicates that the blade-to-blade variations in stress are strongly influenced by factors other than blade structural mistuning.

The first possible factor is hub modal participation in which hub response significantly alters blade response. However, phase data

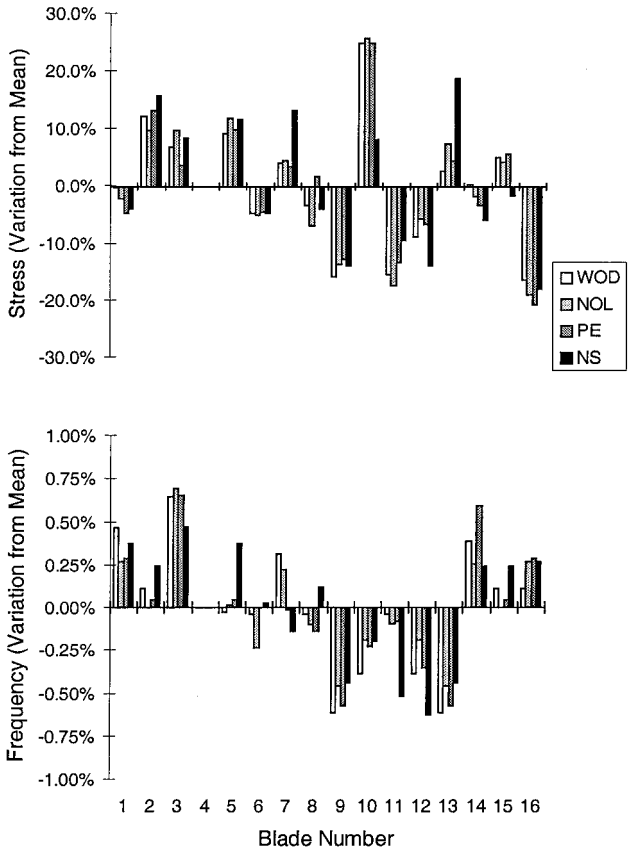

Fig. 5 Blade resonant frequency and stress variations.

from this experiment do not indicate the presence of a hub mode. Interblade phase angle can be expressed mathematically as

$$\sigma_B = -360^\circ(C/N) \tag{1}$$

Solving Eq. (1) for C yields either the engine order of an aerodynamic disturbance or the number of nodal diameters in a hub mode, whichever dominates the response. The negative sign indicates a backward-traveling wave, which occurs in a stable system such as the test rotor. The phase measured from recorded signals between a pair of adjacent blades was approximately −67 deg. From Eq. (1), this measurement indicates a backward-traveling three-nodal wave typical of response to a 3/rev inlet forcing function.

In addition, finite element modeling of the rotor does not support hub participation. Predicted frequencies were plotted vs nodal diameter for a model of the rotor. In this form of analysis, blade modes appear as essentially horizontal lines because the number of nodal diameters does not significantly affect blade stiffness. However, as the number of nodal diameters increase, the disk rapidly becomes stiffer. Therefore, disk or hub modes appear as diagonal lines with frequencies increasing monotonically with nodal diameter. Where these cross, the modal response will veer or turn to show interaction between modes.[10] Figure 6 shows the predicted frequencies plotted vs nodal diameters for the first mode of the rotor in a static condition. Figure 6 shows that modal veering does not occur for the 1F mode. Thus, hub modal participation does not appear to be a major factor in the resonant response at this crossing.

Unsteady aerodynamic coupling is the second possible factor influencing the blisk mistuned response. The blade passage flowfield at this condition is complex, and detailed analysis of the flowfield is beyond the scope of this study. However, stress data from off-resonant conditions at constant speed give some insight here.

The stress variations from the rotor mean are shown in Fig. 7 for all four throttle conditions at 8100 and 9100 rpm. The response at the excitation frequency was measured for each blade. At 8100 rpm this frequency was 405 Hz, and at 9100 rpm the excitation frequency was 455 Hz. The amplitude of the response for each blade at these

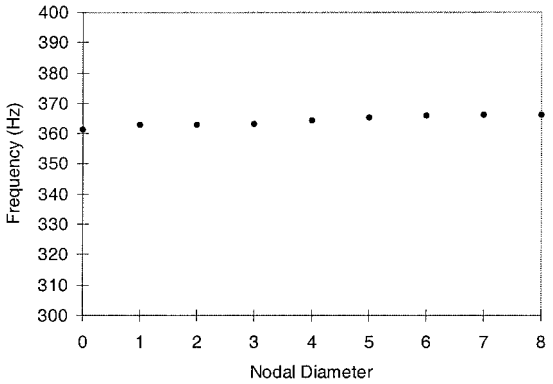

Fig. 6 Frequency vs nodal diameter plot for test rotor 1F mode.

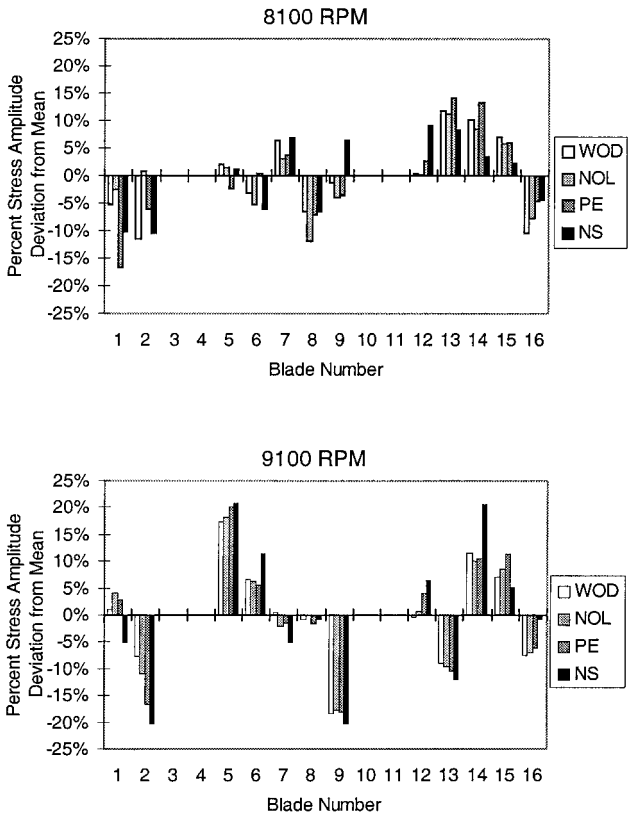

Fig. 7 Off-resonant stress variations.

frequencies varied significantly. At 8100 rpm the stresses varied by as much as 17% of the mean stress at the PE throttle condition, and the standard deviation ranged from 6.7% at NOL to 8.7% at PE. At 9100 rpm the stress amplitude at the forcing frequency varied by up to 21% of the mean while operating near stall, with the standard deviation ranging from 9.8% at WOD to 13.7% at NS.

Figure 7 shows similar patterns between operating lines at constant speed. The blade-to-blade stress distributions at 8100 and 9100 rpm change quantitatively with throttle condition but are qualitatively the same. However, the fundamental pattern changes considerably from one speed to the other, indicating a relationship between speed and blade-to-blade stress distribution, which suggests that blade unsteady aerodynamics are involved. For example, unsteady aerodynamic damping on each blade can vary because of small differences in angle of attack and blade curvature that do not appreciably affect blade structure. At high subsonic Mach numbers, such as those experienced by the blades during the experiment, these differences can account for the variation in blade response around the rotor. As rotor speed changes, blade untwist and changes in the relative flow velocity experienced by the blades may account for the changes in distribution between speeds as seen in Fig. 7.

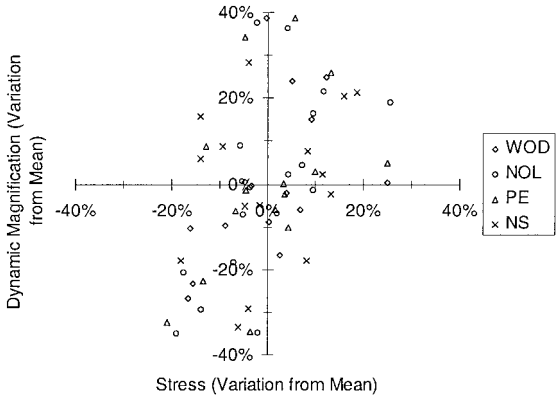

Fig. 8 Correlation of stress and dynamic magnification variations.

This observation is supported by the resonant stress distribution shown earlier in Fig. 5. Whereas these stresses were not measured at a constant speed, resonance occurred at nearly the same operating speed for each throttle condition. The maximum speed difference between operating lines was less than 20 rpm. Therefore, the resonant conditions for each operating line may be assumed to occur at essentially constant speed, comparable to the off-resonant constant speed conditions.

Direct investigation of damping at the resonant condition shows that significant variations were present. Viscous damping was obtained using the half-power method, and then converted to the dynamic magnification factor to clarify comparison to stress variations. The dynamic magnification factor is related to viscous damping by

$$Q = 1/(2\zeta) \tag{2}$$

Figure 8 shows the variations in Q in comparison to the measured resonant stress variations. Figure 8 shows that the variations in Q roughly correspond to the variations in stress amplitude, with the Q variation being approximately double that of stress in many cases. Thus, stress variations show an inverse relationship to damping variations.

In blisks such as the test rotor, structural damping is very small in comparison with aerodynamic damping and is often neglected. Therefore, the damping measured during the experiment may be considered aerodynamic damping. Based on this assumption and the results shown in Fig. 8, the measured stress variations at resonance may be attributed at least in part to variations in aerodynamic damping.

Reduced-Order Model

The effects of unsteady aerodynamic coupling on the forced response of the blisk at its first blade mode were investigated with the reduced-order method developed by Ottarsson et al.[10] and Kruse and Pierre.[11] This method employs a component mode technique with components consisting of disk-induced motion and cantilevered blade motion, allowing individual mistuning of each blade. Blade motion consists of blade finite element mode shapes, with the blade cantilevered at its interface with the disk, superimposed on the motion of the disk. Disk motion is described by finite element mode shapes of the disk with massless blades attached. Finite element modeling of a single disk-blade sector is required to obtain mode shapes. These mode shapes are used to build a reduced-order model of the entire rotor with a reduced number of degrees of freedom in comparison with a complete finite element model. Monte Carlo simulations provide a statistical analysis of frequency variations, which are assumed to be random, and the resulting displacement variations. Motion-dependent aerodynamic coupling can also be incorporated into the model. Output consists of a normalized resonant displacement for each blade, with normalization based on finite element coordinates. Because the model is assumed to be linear, the displacements are proportional to stress, and percent deviations from the circumferential mean displacement can be directly correlated to percent deviations from the mean stress determined experimentally.

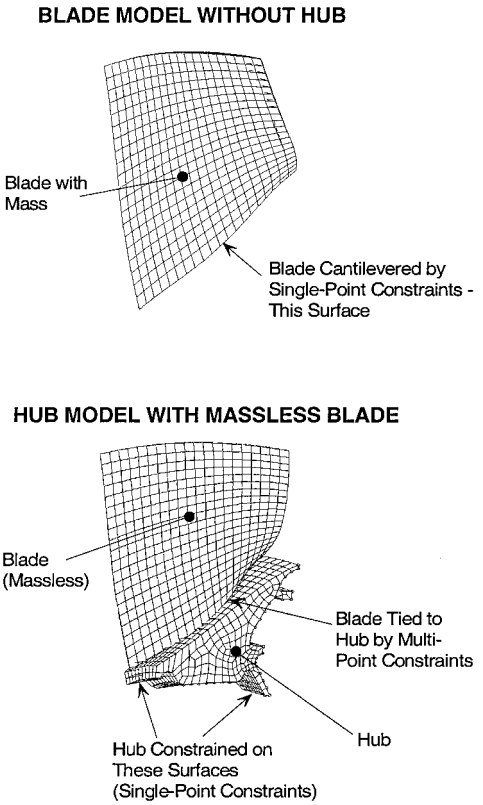

Fig. 9 Rotor finite element models.

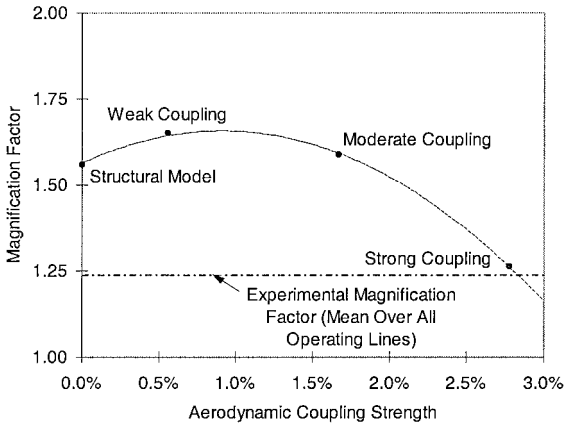

Fig. 10 Predicted magnification factors for various aerodynamic coupling strengths.

The forced response portion of the program has been validated against a full finite element model of an industrial turbomachine rotor.[14]

The structural model of the blisk was based on two finite element models, as shown in Fig. 9. The first consisted of a single hub-blade sector and determined the hub contribution to blade response. The blade portion was comprised of 1200 brick elements and 1764 nodes, and the hub was created using 1098 elements and 1630 nodes. The blade elements were assigned no mass by specifying zero density in the material properties of those elements, and the blade was fixed to the hub surface by multipoint constraints. The attach points of the hub to the compressor main shaft were fixed by single-point constraints on all displacement degrees of freedom.

The reduced-order model requires the use of cyclic symmetry in the hub finite element model, which is based on linear superposition. This precludes direct consideration of centrifugal stiffening, which requires a nonlinear finite element analysis. To account for this result, the hub modulus of elasticity was increased by 34% to reflect centrifugal stiffening. This modulus yielded the same frequency response in a linear blade model as was obtained for the nonlinear blade model with the original modulus.

The second finite element model consisted of the blade alone, cantilevered at its root to solve for the blade mode shapes. The hub elements were removed from this model, and the blade root was fixed using single-point constraints on all displacement degrees of freedom. A nonlinear modal analysis was performed, which yielded blade frequencies and mode shapes with centrifugal stiffening at speed. The predicted blade response frequency in the first mode was 435.5 Hz, which agrees with the experimental results shown in Table 4. This model was also used to determine blade mass and stiffness matrices for the reduced-order model. Blade mistuning parameters used as input to the reduced-order model were based on static bench tests of the blades.[15]

Motion-dependent aerodynamic coupling in the reduced-order model is introduced in the form of a matrix of dimensional unsteady aerodynamic terms. For analysis of the 1F mode in the test rotor, unsteady lift terms were required for the blades.[16] A nondimensional unsteady lift coefficient for each interblade phase angle was obtained from an aerodynamic code developed by Whitehead.[17] This code predicts aerodynamic influence coefficients to account for the effects of the motions of the rotor blades on a given blade based on phase angle relationship. The coefficients were dimensionalized by the lowest eigenvalue from the cantilevered-blade finite element model to obtain lift terms consistent with the reduced-order model. The resulting unsteady terms were reduced by weighting factors of $\frac{1}{180}$, $\frac{1}{60}$, and $\frac{1}{36}$ to consider weak, moderate, and strong aerodynamic coupling, respectively, which follows the convention of the authors of the reduced-order program.[14]

The three aerodynamic coupling strengths were studied to determine the strength of the coupling in the test rotor. Simulations were performed for each coupling strength, with the results expressed in terms of a magnification factor. The magnification factor is the ratio of the largest predicted response to the tuned rotor blade response, which is approximately equivalent to the ratio of the greatest peak blade stress to the mean resonant stress around the rotor. Figure 10 shows the magnification factor predicted for each coupling strength along with the magnification factor from the mistuned structural model with no aerodynamic coupling. The parabolic curve is a second-order polynomial curve fit to observe trends. The experimental magnification factor averaged over all operating lines is provided for comparison.

In Fig. 10 the mistuned structural model with no aerodynamic coupling did not predict the stress variation observed in the test rotor. The predicted magnification factor was 1.56, while a mean magnification factor of 1.24 was measured in the blisk. More succinctly, the predicted variations caused by structural mistuning alone were more than double the measured variations, 56 vs 24%, respectively. In addition, the structural model predicted a correlation between response frequency and amplitude, which is not consistent with the experiment.

With results from the structural model as a baseline, Fig. 10 shows that the displacement variations increase in the blisk with aerodynamic coupling strength to a maximum and then begin to decline. This result is not surprising. A similar trend was determined to generally occur for mistuned systems in a study by Ottarsson and Pierre.[18] They reasoned that a mostly localized response would give some variation from blade to blade, as seen by the result for no aerodynamic coupling. As coupling increases, energy is exchanged between blades, which allows a blade to absorb the energy of its neighbors and vibrate more vigorously, illustrated by the peak in the maximum magnification factor shown in Fig. 10 between weak and moderate aerodynamic coupling. However, increasing coupling further can actually reduce mistuned response because so much energy is shared between blades that the response is no longer localized. Instead, the entire rotor begins to respond as a system.

The predicted magnification factor for strong aerodynamic coupling agreed with experimental data at the blisk 1F mode. As a result, several additional Monte Carlo simulations were performed with strong aerodynamic coupling. The standard deviation of the predicted displacements ranged from 18 to 21% during these simulations, which is somewhat greater than experimental results.

However, the consistent correlation between peak displacement and response frequency no longer existed for each simulation, similar to what was observed during the experiment. Energy transfer through aerodynamic coupling appears to dominate the mistuned response, removing the correlation between resonant amplitude and blade structure. These results indicate that strong aerodynamic coupling likely existed in the blisk during the experiment.

Conclusions

Blade-to-blade variations in resonant frequency, vibratory stress amplitude, and viscous damping in response to an inlet forcing function were measured in a high-speed, low-aspect-ratio blisk. Resonant response of the rotor demonstrated that the blisk was essentially tuned, thus decoupling blade structure from measured blade stress amplitude variations. This finding is particularly important because such stress amplitude variations are classically attributed to blade structural mistuning. Interblade phase angle measured at resonance and results from finite element modeling of the rotor indicated that hub motion was not a significant factor in the measured stress variations. Blade-to-blade stress distribution patterns and lack of correlation with response frequency suggested the presence of strong aerodynamic coupling. Moreover, aerodynamic damping variations were shown to correspond roughly with blade-to-blade stress amplitude variations.

Results from a reduced-order model incorporating unsteady aerodynamic coupling indicated that strong aerodynamic coupling was likely. This coupling could actually reduce localization in the rotor such that blade-to-blade stress variations were less than their possible maximum. Detailed modeling of the rotor with strong aerodynamic coupling showed reasonable agreement with experimental results. The magnitudes of the predicted variations were slightly larger than those measured during the experiment. Thus, the combined experimental and analytical results of this study indicate that the magnitude and distribution of the variations in the test rotor were strongly influenced by aerodynamic loading.

The use of blisks in modern compressor rotor design leads to systems that are more tuned than traditional bladed-disk assemblies. As a result, unsteady blade loads that may be overshadowed by mistuning effects in a bladed-disk assembly become significant in a blisk. More consideration must be given to the role of unsteady aerodynamic coupling in mistuned rotor response, especially as rotor designs continue to advance. Blade-to-blade energy transfer through unsteady aerodynamic loading is not well understood. This investigation shows that an improved understanding of the complex flowfield in the blade passage, and particularly how this facilitates coupling between blades, is necessary to fully characterize blade response variations.

Acknowledgments

The authors would like to thank the staff of the Turbine Engine Research Center and General Electric Aircraft Engines for their many contributions to this effort. We would also like to thank the U.S. Air Force Research Laboratory and General Electric Aircraft Engines for allowing us to publish this work.

References

[1]Whitehead, D. S., "Effect of Mistuning on the Vibration of Turbomachine Blades Induced by Wakes," *Journal of Mechanical Engineering Science*, Vol. 8, No. 1, 1966, pp. 15–21.

[2]Wagner, J. T., "Coupling of Turbomachine Blade Vibrations Through the Rotor," *Journal of Engineering for Power*, Series A, Vol. 89, No. 4, 1967, pp. 502–513.

[3]Dye, R. C. F., and Henry, T. A., "Vibration Amplitudes of Compressor Blades Resulting from Scatter in Blade Natural Frequencies," *Journal of Engineering for Power*, Vol. 91, No. 3, 1969, pp. 182–188.

[4]Ewins, D. J., "Vibration Modes of Mistuned Bladed Disks," *Journal of Engineering for Power*, Vol. 98, Series A, No. 3, July 1976, pp. 349–355.

[5]Kruse, M. J., and Pierre, C., "An Experimental Investigation of Vibration Localization in Bladed Disks, Part I: Free Response," *Proceedings of the International Gas Turbine and Aeroengine Congress and Exhibition*, American Society of Mechanical Engineers, Paper 97-GT-501, June 1997.

[6]Sinha, A., "Calculating the Statistics of Forced Response of a Mistuned Bladed Disk Assembly," *AIAA Journal*, Vol. 24, No. 11, 1986, pp. 1797–1801.

[7]Sinha, A., and Chen, S., "A Higher Order Technique to Compute the Statistics of Forced Response of a Mistuned Bladed Disk," *Journal of Sound and Vibration*, Vol. 130, No. 2, 1989, pp. 207–221.

[8]Ottarsson, G. S., and Pierre, C., "Vibration Localization in Mono- and Bi-Coupled Bladed Disks—A Transfer Matrix Approach," AIAA Paper 93-1492, 1993, pp. 3683–3697.

[9]Kaza, K. R. V., and Kielb, R. E., "Effects of Structural Coupling on Mistuned Cascade Flutter and Response," *Journal of Engineering for Gas Turbines and Power*, Vol. 106, No. 1, 1984, pp. 17–24.

[10]Ottarsson, G. S., Castanier, M. P., and Pierre, C., "A Reduced-Order Modeling Technique for Mistuned Bladed Disks," AIAA Paper 94-1640, 1994, pp. 2552–2562.

[11]Kruse, M. J., and Pierre, C., "Forced Response of Mistuned Bladed Disks Using Reduced-Order Modeling," AIAA Paper 96-1545, 1996, pp. 1938–1950.

[12]Griffin, J. H., "On Predicting the Resonant Response of Bladed Disk Assemblies," *Journal of Engineering for Gas Turbines and Power*, Vol. 110, No. 1, 1988, pp. 45–50.

[13]Nichol, K. L., "Numerical Strain Gage Representation," AIAA Paper 98-1720, AIAA, Reston, VA, 1998, pp. 198–203.

[14]Kruse, M. J., and Pierre, C., "Dynamic Response of an Industrial Turbomachine Rotor," AIAA Paper 96-2820, July 1996.

[15]Minkiewicz, G., and Russler, P., "Dynamic Response of Low Aspect Ratio Blades in a Two Stage Transonic Compressor," AIAA Paper 97-3284, July 1997.

[16]Pierre, C., Castanier, M. P., and Bladh, R., "REDUCE Version 2.1 User's Manual," Dept. of Mechanical Engineering and Applied Mechanics, Univ. of Michigan, Ann Arbor, MI, 1997.

[17]Whitehead, D. S., "Classical Two-Dimensional Methods," *AGARD Manual on Aeroelasticity in Axial Flow Turbomachines, Volume 1: Unsteady Turbomachine Aerodynamics*, AGARD-AG-298, Vol. 1, 1987, Chap. III.

[18]Ottarsson, G., and Pierre, C., "On the Effects of Interblade Coupling on the Statistics of Maximum Forced Response Amplitudes in Mistuned Bladed Disks," AIAA Paper 95-1494, April 1995, pp. 3070–3078.